

## de Haas-van Alphen and Galvanomagnetic Effect in Bi and Bi-Pb Alloys

R. N. BHARGAVA\*

IBM Watson Laboratory, Columbia University, New York, New York

(Received 17 October 1966)

The de Haas-van Alphen (dHvA) effect in pure Bi and lightly doped Bi-Pb alloys was studied using a sensitive mutual-induction technique. In pure Bi, we obtained for the electron and hole Fermi surfaces, respectively: Fermi energies  $E_n=25.0$  meV and  $E_p=11.0$  meV; the number densities per ellipsoid  $n=0.96 \times 10^{17}/\text{cc}$  and  $p=3.00 \times 10^{17}/\text{cc}$ , and the Dingle temperatures  $\kappa_n=0.68^\circ\text{K}$  and  $\kappa_p=0.2^\circ\text{K}$ . Additionally, we find that for the conduction band the energy dispersion in the heavy-mass direction is essentially the same as in the lighter-mass direction; i.e., the constant-energy surfaces are very closely ellipsoidal. The data on Bi-Pb alloys show that the relative motion of the conduction and the overlapping valence band is negligible and only the Fermi level shifts with alloying. From the dHvA and the galvanomagnetic data in Bi-Pb alloys in moderate fields, we deduced that the electron and hole mobilities decrease inversely as  $(N_p-N_n)$  as expected, where the  $N$ 's are the total carrier densities and we assume that all the Pb atoms scatter independently as ionized impurities.

### I. INTRODUCTION

THE de Haas-van Alphen (dHvA) effect, first observed in Bi,<sup>1</sup> provides a powerful tool for mapping the Fermi surface topology. A simple relation, due to Onsager<sup>2</sup>

$$P(1/H) = (2\pi e/\hbar c)1/S \quad (1)$$

gives  $P$ , the period of the dHvA oscillations in units of reciprocal gauss, in terms of  $S$ , the extremal cross-sectional area in  $\text{cm}^{-2}$  of the Fermi surface normal to the field direction.

The dHvA effect is usually observed by either a torque<sup>3</sup> or a pulsed-field<sup>4</sup> method. In the torque method, advantage is taken of the tensor character of the susceptibility. The magnetization of a sample, usually at an angle to the applied field, is measured by observing the resulting torque with a torsion balance. This method is frequently used for multivalent metals and semimetals. The main drawback of this method is that the torque contribution of a particular part of the Fermi surface vanishes when the magnetic field is normal to an "eigenarea," i.e., a high-symmetry cross section of the surface. These eigenareas, often the main information desired, must then be obtained by extrapolation, frequently with erroneous results. Additionally, the torque vanishes for certain orientations determined by the crystal symmetry. The pulsed-field method is used for good metals where a typical period is  $\sim 10^{-9}$  G<sup>-1</sup> because of the large Fermi surface dimensions, necessitating high fields. The effect is observed by the induction in a pickup coil produced by the time-varying

magnetization. While the pulsed-field method can be used to observe bigger areas, it is limited by low resolution, eddy currents, and thermal instability to periods above  $10^{-7}$  G<sup>-1</sup>.<sup>4</sup>

To resolve uncertainties in the Bi-Fermi surface, we require accurate measurements of the eigenareas corresponding to periods ranging from  $10^{-6}$  to  $10^{-4}$  G<sup>-1</sup>, for which neither method is well suited. In view of the above, we used a sensitive mutual<sup>5</sup> induction method which can measure periods over this range, in all directions. The method, particularly suitable to low conductivity materials, has been successfully applied to map the entire Fermi surface of Bi accurately and to study the changes in the Fermi surface when Bi is doped with small quantities of Pb. Similar techniques have been used recently by other authors<sup>6-8</sup> for other specific applications.

Early results showed<sup>3,9,10</sup> that the Fermi surface for electrons in Bi could be approximated by a set of equivalent ellipsoids in momentum space, with one principal axis of each ellipsoid parallel to a crystal axis of twofold rotational symmetry (binary) and the other two tilted about  $6^\circ$  from the trigonal and bisectrix axes. Experimental<sup>11-15</sup> and theoretical<sup>11,16,17</sup> work in recent years has shown that the energy-momentum dispersion

\* R. N. Bhargava, Bull. Am. Phys. Soc. **10**, 605 (1965).

<sup>6</sup> D. Shoenberg and P. J. Stiles, Proc. Roy. Soc. (London) **A281**, 62 (1964).

<sup>7</sup> A. Goldstein, S. J. Williamson, and S. Foner, Rev. Sci. Instr. **36**, 1356 (1965).

<sup>8</sup> L. R. Windmiller, Phys. Rev. **149**, 472 (1966).

<sup>9</sup> H. Jones, Proc. Roy. Soc. (London) **A147**, 396 (1934); M. Blackman, *ibid.* **A166**, 1 (1938).

<sup>10</sup> B. Abeles and S. Meiboom, Phys. Rev. **101**, 544 (1956).

<sup>11</sup> B. Lax, Bull. Am. Phys. Soc. **5**, 167 (1960); B. Lax, J. G. Mavroides, H. J. Zeiger, and R. J. Keyes, Phys. Rev. Letters **5**, 241 (1960).

<sup>12</sup> Richard N. Brown, J. G. Mavroides, and B. Lax, Phys. Rev. **129**, 2055 (1963).

<sup>13</sup> W. E. Engeler, Phys. Rev. **129**, 1509 (1963).

<sup>14</sup> D. Weiner, Phys. Rev. **125**, 1226 (1962).

<sup>15</sup> Y. H. Kao, Phys. Rev. **129**, 1122 (1963).

<sup>16</sup> M. H. Cohen, Phys. Rev. **121**, 387 (1961).

<sup>17</sup> A. L. Jain and S. H. Koenig, Phys. Rev. **127**, 442 (1962).

\* Present address: T. Watson Research Center, Yorktown Heights, New York.

<sup>1</sup> W. J. de Haas and P. M. van Alphen, Proc. Acad. Sci. Amsterdam **33**, 1106 (1930).

<sup>2</sup> L. Onsager, Phil. Mag. **A250**, 325 (1952).

<sup>3</sup> D. Shoenberg, *Progress in Low-Temperature Physics* (North-Holland Publishing Company, Amsterdam, 1957), Vol. II and the references mentioned therein.

<sup>4</sup> D. Shoenberg, Phil. Trans. Roy. Soc. (London) **A255**, 85 (1962).

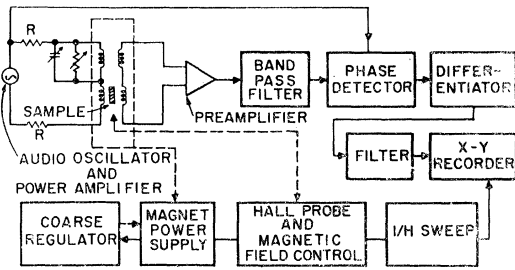


FIG. 1. Block diagram of dHvA measuring apparatus.

relation for the electrons is not quadratic and that the electron Fermi surface should differ somewhat from an ellipsoidal shape. By mapping out the Fermi surface using dHvA effect we conclude that any such deviation in pure Bi is in fact very small. That the Fermi surface for holes in Bi possesses the symmetry of an ellipsoid of revolution about the trigonal axis,<sup>9,15,18</sup> known to be for sometime, is established with greater certainty than in any other previous work.

The conduction and valence bands in Bi overlap; immediately below the conduction band, there lies another valence band of similar symmetry separated by energy gap  $E_g \sim 15$  meV. The band structure of Bi below and above the Fermi level has been previously investigated by doping it with Sn, Pb, As, Sb, and Te. The early work of Thompson,<sup>19</sup> and Shoenberg and Uddin<sup>20</sup> had been of an exploratory nature. Since then a reasonable amount of work has been done on various Bi-alloys. Weiner<sup>14</sup> in Bi-Te and Brandt *et al.* in Bi-Pb<sup>21</sup> and Bi-Sb<sup>22,23</sup> alloys used dHvA effect to study the conduction band. The present study of Bi-Pb alloys was undertaken in order to (i) make possible judgments about the energy-momentum dispersion relation of the electrons by noting the change of the extremal momenta in all directions as the Fermi energy decreases with increasing concentration of Pb, (ii) observe the change of the Fermi level and obtain the relative shift in the position of the conduction and the valence bands, if any, (iii) to obtain the change in electron and hole concentration produced per atom of Pb added.

The value of the carrier concentration change  $\Delta \equiv N_p - N_n$ ,  $N_p$  and  $N_n$  being the hole and electron concentrations, respectively, in various alloys can be obtained without the dHvA effect, by a study of the resistivity and Hall coefficient as a function of magnetic field  $H$ , chosen such that  $\mu H \gg 1$ , but still sufficiently low that

<sup>18</sup> R. D. Brown, Bull. Am. Phys. Soc. **9**, 264 (1964).

<sup>19</sup> N. Thompson, Proc. Roy. Soc. (London) **A155**, 111 (1936); **A164**, 24 (1938).

<sup>20</sup> D. Shoenberg and M. Z. Uddin, Proc. Roy. Soc. (London) **A156**, 687 (1936).

<sup>21</sup> N. B. Brandt and M. V. Razumeenko, Zh. Eksperim. i Teor. Fiz. **39**, 276 (1960) [English transl: Soviet Phys.—JETP **12**, 198 (1961)].

<sup>22</sup> N. B. Brandt and V. V. Shchekochikhina, Zh. Eksperim. i Teor. Fiz. **41**, 1412 (1961) [English transl: Soviet Phys.—JETP **14**, 1008 (1962)].

<sup>23</sup> Y. H. Kao, R. D. Brown, and R. L. Hartman, Phys. Rev. **136**, A858 (1964).

quantum effects remain small. It was originally hoped that the galvanomagnetic measurements would serve as an independent check on  $\Delta$ . However, the dHvA values turned out to be more accurate. Combining then the dHvA and galvanomagnetic data, the electron and hole mobilities as a function of doping were obtained.

## II. EXPERIMENTAL PROCEDURE

### A. Apparatus

Figure 1 shows the block diagram of the apparatus used for observing the dHvA effect. The differential susceptibility of a sample is measured with the help of a pair of balanced mutual inductors. Two identical secondary coils, each about 8000 turns of No. 44 copper wire wound in an approximate area of  $1 \text{ cm}^2$  on a Teflon frame, are connected in series opposition. They are driven at 500 cps by two separate identical primary coils connected series aiding, each with 108 turns of No. 34 copper wire. If the two mutual inductors and their environments are identical there should be no secondary voltage output. Under such circumstances, if a sample is placed in one of the secondary coils, an unbalanced voltage is developed in the secondary

$$E = [4\pi\alpha AN(dH_{\text{osc}}/dt) \times 10^{-8}] (dI/dH) \text{ volts,} \quad (2)$$

where  $A$  and  $N$  are, respectively, the cross-sectional area and an effective number of turns for one of the secondary coils;  $\alpha$  is a filling factor,  $H_{\text{osc}}$  the field produced by the primary and  $dI/dH$  the differential susceptibility of the sample. The quantity inside the square brackets in Eq. (2) is the voltage picked up by one of the secondary coils and can be measured separately. Thus in principle, we can also measure the absolute value of  $dI/dH$ . The oscillations in  $dI/dH$  can be recorded by amplifying and synchronously phase-detecting the secondary output  $E$  at the driving frequency as the magnetic field  $H$  is swept.

The magnetic field is swept in such a way that  $1/H$  is linear in time.<sup>18</sup> The sweep circuitry, which will be discussed in detail by Brown elsewhere,<sup>24</sup> involves (i) generating a sweep voltage the reciprocal of which varies linearly in time and (ii) comparing this voltage with the output of a linearized Hall probe voltage and feeding the difference to the null detector of the magnet supply current regulator. Sweeping the field such that  $1/H$  is linear in time produces dHvA oscillations sinusoidal in time, enabling one to differentiate or to filter the real time signal when useful. This provides an easier method to analyze the data as compared to plotting ordinal numbers of maxima and minima versus the calculated values of  $1/H$ . More than that, it prevents falsely assigning meaning to peaks which are really the accidental result of beating periods.

<sup>24</sup> R. D. Brown, IBM J. Res. Develop. **10**, 462 (1966).

The secondary output first goes to a low-noise Keithley 103R preamplifier, then to a variable band-pass filter (to prevent noise from overloading the following stages) and finally to a narrow-band lock-in-amplifier similar to an Electronics, Missiles and Communications, Ltd., Model RJB, where it is synchronously phase-detected. The output of the phase detector feeds to the  $y$  axis of a Varian F-80  $x$ - $y$  recorder. The  $x$  axis of the recorder is driven by the voltage which is the source of the  $1/H$  sweep signal.

A 12-in. Varian electromagnet with  $3\frac{1}{4}$ -in. gap producing fields up to 13.5 kG was used. The field was calibrated at 10 and 5 kG using nuclear magnetic resonance.

In practice, the primary and secondary coils as well as the coupling between the secondaries is not identical. A resistance-capacitance shunt across one of the primary coils enables one to compensate for this residual coil unbalance to one part in  $10^6$ . The noise is typically of the order of ten times the unbalance signal, or  $\sim 10$ - $\mu$ V peak-to-peak for a bandwidth between 100 to 1000 cps at magnetic fields  $\sim 10$ kG. However, most of this noise is integrated out in the lock-in-amplifier. This noise is mainly from mechanical vibrations which alter the balance conditions. This noise which was minimized by having rigid supports and choosing the primary drive frequency so as not to coincide with a structural resonance, remained the factor limiting the sensitivity of the apparatus. Residual fluctuations of the well regulated field ( $1$  in  $10^6$ )  $H_N$ , picked up by the coils, become significant at the higher fields. This noise as compared to the signal could be reduced, if necessary, by having additional regulation in the field and by driving the primaries at higher currents. The limit of course is that  $H_{osc}$  should be less than the interval  $\Delta H$  between two consecutive dHvA oscillations. The other noise sources, considerably smaller, are Johnson noise, of approximately  $5 \times 10^{-4}$   $\mu$ V for the system, and the input noise equivalent of the preamplifier, approximately  $0.1$   $\mu$ V for a bandwidth of 10 cycles, compared to vibration noise  $\simeq 1$   $\mu$ V for this bandwidth. From Eq. (2) and an estimate of  $dI/dH$  from Eq. (3) below, we expect values of the signal  $E$  of  $\sim 500$  and  $5\mu$ V for the small and large areas of the Bi-Fermi surface at  $1.3^\circ$ K in good agreement with the observed dHvA oscillation amplitudes.

The balance conditions for zero output on the secondary side change appreciably as the magnetic field is swept, for two reasons: (i) since one of the primary coils is shunted, a change in resistance of these coils will change the balance conditions. The changing magnetoresistance of the coils causes significant unbalance as the field is swept. (ii) The permeability of the iron core decreases at high fields, altering both the primary-secondary coupling and the inductance, somewhat differently for each set of coils, thereby causing an offset in the balance conditions. These two factors have greater effect as the angle  $\theta$  between the coil axis and magnetic field is increased. Such off-balance produces a dc shift

at the output of the phase detector, causing the trace on the  $x$ - $y$  recorder to move off scale. This was minimized when necessary by differentiating the phase detector output. It is difficult to assess the improvement in sensitivity of the above technique over the usual method. For Bi, however, we report here for the first time the electron periods along the trigonal directions, and have observed hole periods at lower fields and higher temperatures than reported previously.

### B. Sample Preparation

Bismuth of 99.9999% purity was purchased from Consolidated Mining and Smelting Company of Canada, Ltd. It was zone refined several times under vacuum in a carbon-coated quartz boat approximately  $30 \text{ cm} \times 2.5 \text{ cm} \times 1 \text{ cm}$  and allowed to grow from one end. Typically, single crystals were obtained for the full length of the boat. A piece was cut from the central portion of the ingots by a Servomet spark cutter and etched in 33% nitric acid. The trigonal surfaces were obtained by cleaving under liquid nitrogen. A  $\frac{1}{4}$ -in. cubical sample was cut by aligning the square cutter with the binary slip lines under a microscope.

For Bi-Pb alloys, a master alloy was first prepared by zone leveling known amounts of Bi and Pb. Successive dilution was used to obtain the desired concentrations. After zone leveling four to five times, the charge is left to grow from one end, as for pure Bi. The samples were near to this end. The amount of Pb in various alloys, determined by quantitative emission spectroscopy,<sup>25</sup> within  $\pm 10\%$ , is listed in column 2 of Table VI.

The samples for galvanomagnetic effects were cut from the cubic single crystals used for dHvA measurements. Typical samples sizes were  $6.5 \text{ mm} \times 2.0 \text{ mm} \times 2.0 \text{ mm}$ . The current was along the binary (length), the transverse magnetic field  $H$  in the direction of the trigonal axis and the Hall contacts in the bisectrix direction.

### C. Sample Alignment

The effective magnetic susceptibility  $\chi$  of a sample can be written as  $\chi = \chi_1 + i\chi_2$ , where  $\chi_1$  is the real magnetic susceptibility and  $\chi_2$  the absorptive part, in our case related to eddy-current losses in the sample. If the primaries of the pickup coil are driven at 8 Kc/sec, the contribution of  $\chi_2$  is greater than  $\chi_1$  at  $4.2^\circ$ K and low magnetic fields. The eddy-current losses depend on the magnetoresistance of the sample which Mase *et al.*<sup>26</sup> have shown to have maxima and minima as one goes from the bisectrix to the binary axes in the trigonal plane. Distinct minima are observed in the pickup-coil signal every  $60^\circ$  which coincide with the binary axis and enable one to align the sample to within  $1^\circ$ .

However, the final, most accurate alignment of the sample is by the dHvA effect, because the periods from

<sup>25</sup> N. W. H. Addink *et al.*, Appl. Spectry, **10**, 128 (1956).

<sup>26</sup> S. Mase, S. von Molnar, and A. W. Lawson, Phys. Rev. **127**, 1030 (1962).

TABLE I. Comparison of the oscillatory periods reported in Bi.

Investigator \ Axis	Electron periods in $10^{-5} \text{ G}^{-1}$			Hole periods in $10^{-5} \text{ G}^{-1}$		
	Binary	Bisectrix	Trigonal	Binary	Bisectrix	Trigonal
Shoenberg <sup>a</sup>	7.4	4.3	1.18 <sup>b</sup>			
Brandt <i>et al.</i> <sup>c</sup>	0.25	8.5		0.46		1.56
	0.48	4.3	1.2 <sup>b</sup>			
Steele and Babiskin <sup>d</sup>	7.1	8.2	1.57			
	0.30	4.1				
Lerner <sup>e</sup>	6.8	4.0	1.2 <sup>b</sup>			1.54
	0.50	7.8				
Brown <sup>f</sup>	7.05	4.1			0.48	1.58
	0.52	8.2				
Eckstein and Ketterson <sup>g</sup>	7.6	4.5		0.50	0.50	1.6
		8.9				
Present	7.20	4.17	1.17		0.45	1.575
	0.53	8.30				

<sup>a</sup> See Ref. 3.<sup>b</sup> Ellipsoidal model-extrapolated value.<sup>c</sup> See Ref. 29.<sup>d</sup> M. C. Steele and J. Babiskin, Phys. Rev. **98**, 359 (1955).<sup>e</sup> See Ref. 30.<sup>f</sup> See Ref. 18.<sup>g</sup> Y. Eckstein and J. B. Ketterson, Phys. Rev. **137**, A1777 (1965).

different ellipsoids combine to form a simple pattern only for  $\mathbf{H}$  along the binary, bisectrix, or trigonal axes. If the coil is aligned such that  $\theta=0$  for  $\mathbf{H} \parallel$  binary or bisectrix, the trigonal axis can be located by looking at the intersection of the two branches of the electron periods (see Fig. 7). This way the uncertainty in the alignment is kept less than  $0.5^\circ$ .

### D. Theoretical Considerations

The detailed computations<sup>27</sup> show that the differential susceptibility  $dI/dH$  can be written as

$$\frac{dI}{dH} = \frac{4kT}{H^{5/2}P^2} \left( \frac{2\pi e}{hc} \right)^{3/2} \left| \frac{1}{2\pi} \frac{\partial^2 S}{\partial K_H^2} \right|^{-1/2} \left\{ \cos\theta - \frac{1}{P} \frac{\partial P}{\partial \theta} \sin\theta \right\} \\ \times \sum_{p=1}^{\infty} p^{1/2} \cos\left( \frac{2\pi p}{HP} - \frac{\pi}{4} - 2\pi p\gamma \right) \cos \frac{\pi p m^*}{m_0} \\ \times \exp \left[ \frac{-4\pi^3 p m^* c k \kappa}{ehH} \right] / \sinh \left[ \frac{4\pi^2 p m^* c k T}{ehH} \right]. \quad (3)$$

$I$  is the oscillatory magnetization per unit volume at angle  $\theta$  to the applied field,  $m^*$  is the cyclotron mass defined as  $m^* = (\hbar^2/2\pi)(\partial S/\partial E)$ , where  $S$  is the extremal area and the derivative is evaluated at the Fermi surface,  $\kappa$  is an effective temperature<sup>28</sup> which takes account of the broadening of the Landau levels. If the level broadening is only due to collisions

$$\kappa = \hbar/\pi k\tau, \quad (4)$$

where  $\tau$  is the mean collision time. The factor  $\cos(2\pi p m^*/m_0)$  which comes from spin splitting of the energy levels<sup>28</sup> is an approximation which holds very

<sup>27</sup> I. M. Lifshitz and A. M. Kosevich, Zh. Eksperim. i Teor. Fiz. **29**, 730 (1955) [English transl: Soviet Phys.—JETP **2**, 636 (1956)].

<sup>28</sup> R. B. Dingle, Proc. Roy. Soc. (London) **A211**, 500 (1952); **A211**, 517 (1952).

well for the magnetic field values used in the experiment. The factor

$$\cos\theta - (1/P)(dP/d\theta) \sin\theta \quad (5)$$

takes into account the components of magnetization parallel and perpendicular to the magnetic field  $H$ . These two terms are used very effectively to separate the periods coming from various pieces of the Fermi surface. If  $\theta \sim 90^\circ$ , the  $\cos\theta$  contribution is negligible; then, only those pieces of the Fermi surface contribute which have nonzero  $dP/d\theta$ . We shall discuss the various regions in Bi-Fermi surface where this factor is utilized to advantage to measure dHvA periods, some of which have never been previously observed.

For the majority of our measurements

$$4\pi^3 m^* c k T / ehH \geq 1$$

applies; it is then reasonable to retain only the first term of the summation in Eq. (3) and replace  $\sinh$  by an exponential. If in the range of magnetic fields used, we can neglect the contribution from the higher harmonics, then the field and temperature dependence of the amplitude  $dI/dH$  appears only through the factor

$$TH^{-5/2} \exp\{-4\pi^3 m^* c k (T + \kappa) / ehH\}. \quad (6)$$

One may then determine the effective mass  $m^*$  from the temperature dependence of the amplitude and then the Dingle temperature from the field variation of the amplitude.

## III. EXPERIMENTAL RESULTS

### A. Bismuth

The dHvA oscillations were recorded as a function of the direction of the magnetic field as it was rotated in the three crystallographic planes. The bulk of the data was taken at  $1.3^\circ\text{K}$ .

The periods corresponding to the electron and hole Fermi surface of Bi have been reported by many

TABLE II. Summary of results of dHvA effect in Bi.

Axes	Electrons			Holes		Electrons	
	Periods in $10^{-5} G^{-1}$ Crystal axis	Periods in $10^{-5} G^{-1}$ Ellipsoidal axis	Area in $10^{12} cm^{-2}$ ellipsoidal axis	Periods in $10^{-5} G^{-1}$	Area in $10^{12} cm^{-2}$	Measured value of $m^*/m_0$ in ellipsoidal axis <sup>a</sup>	$(S/2\pi m^*)$ in the ellipsoidal axis
1	$0.53 \pm 0.03$ $7.20 \pm 0.05$	$0.53 \pm 0.03$	18.0	$0.45 \pm 0.02$	21.2	$0.14 \pm 0.02$	$15.60 \pm 2.8$
2	$8.30 \pm 0.05$ $4.17 \pm 0.05$	$8.35 \pm 0.05$	1.1	$0.45 \pm 0.02$	21.2	$0.009 \pm 0.0009$	$15.40 \pm 1.6$
3	$1.17 \pm 0.03$	$0.695 \pm 0.03$	13.7	$1.575 \pm 0.005$	6.1	$0.11 \pm 0.01$	$15.20 \pm 2.3$
						Average	15.4

<sup>a</sup> As measured by Kao, Ref. 15.

workers (cf. Table I). In no previous measurements have the electron periods been observed in the shaded area of Fig. 3. This is, as explained later, because of the large Dingle temperature. Periods previously reported in this region were obtained by extrapolating the data taken in other directions assuming an ellipsoidal Fermi surface; such an extrapolation cannot, of course, make any comment on the nonellipsoidicity<sup>16</sup> expected in the electron Fermi surface. A major purpose of this study is to determine the periods in the shaded area in Fig. 3, as well as the periods in all other directions more precisely than previously reported, in order to observe deviations from an ellipsoidal surface, if any. Measurements on the hole periods we report, (taken at 1.3°K) show far less scatter and extend over a wider range of  $H$  than that of Brandt *et al.*<sup>29</sup> taken at 0.1°K and below using a torque method, indicating the relative sensitivity of the two experiments, the only two that report dHvA data for holes.

The data in each plane will be considered for electrons and holes separately. The angular variation of electron periods in the various planes is plotted assuming a tilted ellipsoidal model having a tilt of  $6.5^\circ$  and our measured values of eigen periods along the crystal axes<sup>30</sup> tabulated in column 2 of Table II. The plots so obtained are shown by continuous lines in Figs. 2, 3, and 7, and can be used for guidance in following the data presentation. Similarly the plot for the angular dependence of the periods of the hole ellipsoid in the binary plane is shown in Fig. 8 by continuous lines. We designate binary, bisectrix, and trigonal crystal axes as  $X$ ,  $Y$ , and  $Z$ , respectively.

### 1. Electrons

(a)  $H$  in the Trigonal Plane. For  $\mathbf{H} \parallel X$ ,  $\theta = 0$ . Figure 2 shows the data in this plane. We observe two periods of  $0.53 \times 10^{-5}$  and  $7.2 \times 10^{-5} G^{-1}$  in the binary direction. The short periods are obtained from high-field differentiated data.

<sup>29</sup> N. B. Brandt, T. F. Dolgolenko, and N. N. Stupochenko, Zh. Eksperim. i Teor. Fiz. 45, 1319 (1963) [English transl: Soviet Phys.—JETP 18, 908 (1964)] and the references mentioned therein.

<sup>30</sup> Cf. L. S. Lerner, Phys. Rev. 127, 1480 (1962); 130, 605 (1963).

(b)  $H$  in the Binary Plane. For  $\mathbf{H} \parallel Y$ ,  $\theta = 0$ . Figure 3 shows the data in this plane. Electron periods were never observed previously in the shaded region around the trigonal axis because the hole contribution is much greater than the electron contribution. However, if the coils are aligned along the bisectrix, the electron periods in the entire plane can be measured without interference from the presence of holes as shown in Fig. 4. This is due to the presence of the cross term  $(1/P)(dP/d\theta) \sin\theta$  in Eq. (5). In the region around the trigonal axis  $\theta \approx 90^\circ$ ,  $dP/d\theta \approx 0$  for the holes and nonzero for the electrons.

For  $\mathbf{H} \parallel Z$ ,  $\theta = 0$ . In the trigonal direction only holes are observed as shown in Fig. 5. Moving away from the trigonal direction we get beats between the hole periods and the electron periods. Though the hole periods dominate in this region, we accentuate the beating pattern

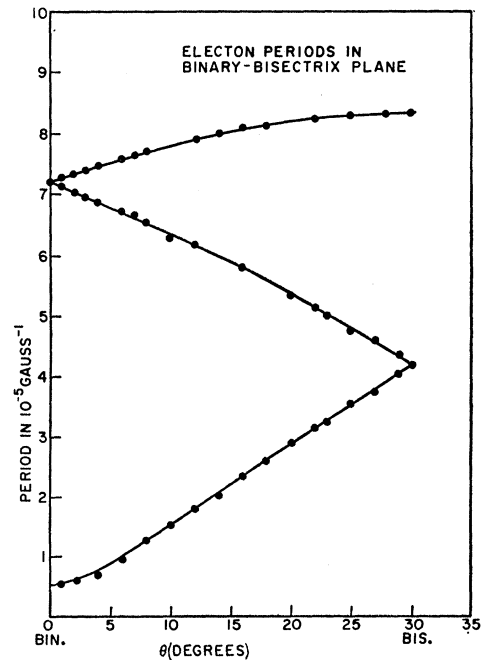


FIG. 2. The angular dependence of electron dHvA periods  $P$  in the trigonal plane for pure Bi. The solid line is a fit assuming an ellipsoidal Fermi surface and using the measured values of periods in the crystal axis and a tilt angle of  $6.5^\circ$ .

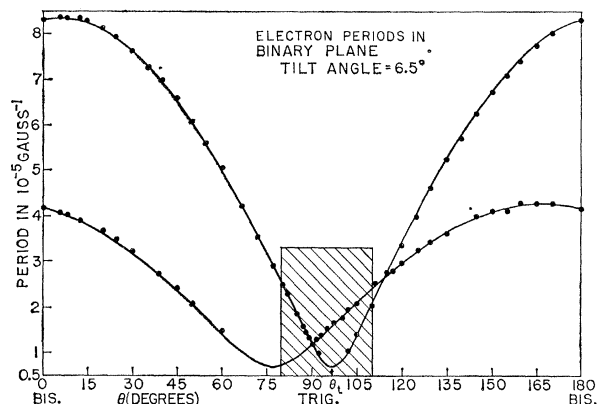


FIG. 3. The angular dependence of electron dHvA periods in the binary plane. The tilt angle measured is  $6.50 \pm 0.25^\circ$ . The shaded area shows the region where electron periods were never reported. The solid line is a fit using an ellipsoidal Fermi surface as in Fig. 2.

by tuning the filter to the electron period as shown in Fig. 6. We can get electron periods more accurately by rejecting the hole periods in this region and differentiating the output of the filter.

(c) *H* in the Bisectrix Plane. For  $\mathbf{H} \parallel X$ ,  $\theta = 0$ . Figure 7 shows the data in this plane. While rotating towards the trigonal axis the upper branch always dominates, so much so that within  $\pm 15^\circ$  of the trigonal, we observe only the upper branch as shown in Fig. 7. Just at the

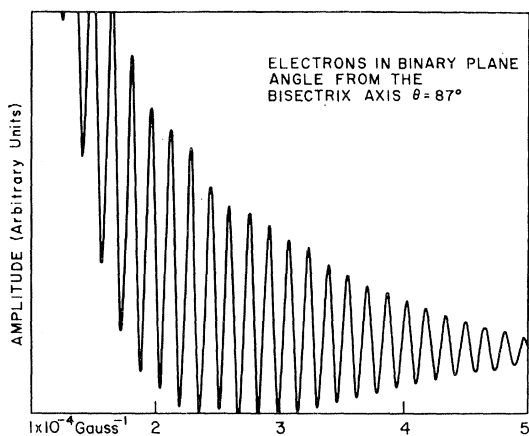


FIG. 4. The differentiated data showing electron periods in the binary plane.  $\theta = 0$  corresponds to the coil axis aligned along the bisectrix direction.

trigonal direction the fundamental period disappears and only the second harmonic is observed. This happens because  $(1/P)(dP/d\theta)$  of the two branches are now equal and opposite in sign, but the second harmonics of the two branches are still in phase. The symmetry of the data makes it possible to determine the trigonal axis accurately.

For  $\mathbf{H} \parallel Z$ ,  $\theta = 0$ . The hole oscillations dominate as in the case  $\mathbf{H} \parallel Z$  in the binary plane.

## 2. Holes

The data for holes are shown in Fig. 8.

For  $\mathbf{H} \parallel Z$ ,  $\theta = 0$ . For both the binary and bisectrix plane we obtain the same results. The measured period in the trigonal direction is  $1.575 \pm 0.005 \times 10^{-5} \text{ G}^{-1}$  determined by averaging over a large number of periods. The holes could be followed as far as  $\pm 75^\circ$  from the trigonal axis in the differentiated data at high fields.

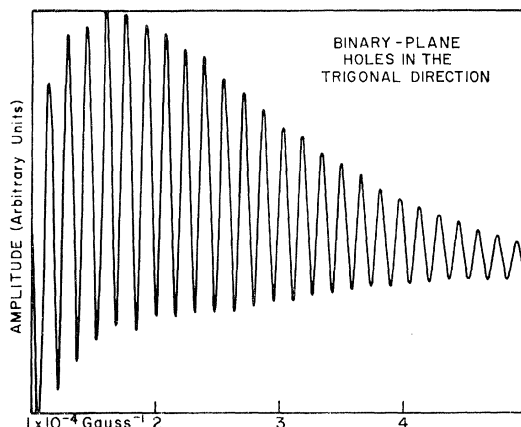


FIG. 5. The differentiated data showing hole periods in the trigonal direction when  $\theta = 0$ . The period is  $1.575 \pm 0.005 \times 10^{-5} \text{ G}^{-1}$ . No electrons are seen.

For  $\mathbf{H} \parallel Y$ ,  $\theta = 0$ . In the trigonal plane we observe a hole period of  $0.45 \pm 0.02 \times 10^{-5} \text{ G}^{-1}$ , independent of orientation which agrees well with the measurements of Brown<sup>18</sup> (cf. Table I).

## B. Bismuth-Lead Alloys

Since Pb in Bi acts as an acceptor we expect to decrease the electron and increase the hole concentration as a function of Pb doping. This is what is found for a series of five samples with Pb concentrations ranging

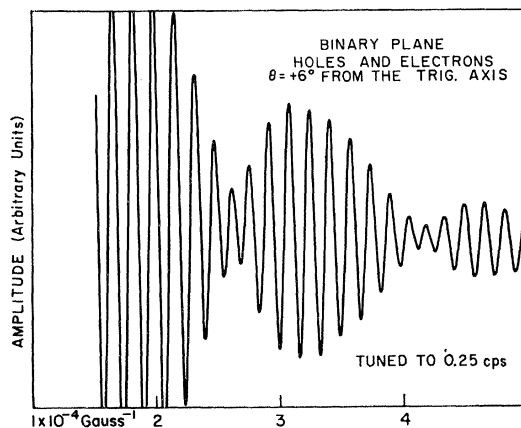


FIG. 6. The beat obtained from hole and electron periods in the binary plane for  $\theta = +6^\circ$  from the trigonal. The hole and electron periods are  $1.57 \times 10^{-5} \text{ G}^{-1}$  and  $1.65 \times 10^{-5} \text{ G}^{-1}$ , respectively. The beating pattern is accentuated by tuning the differentiator output to the electron frequency  $\approx 0.25 \text{ cps}$ .

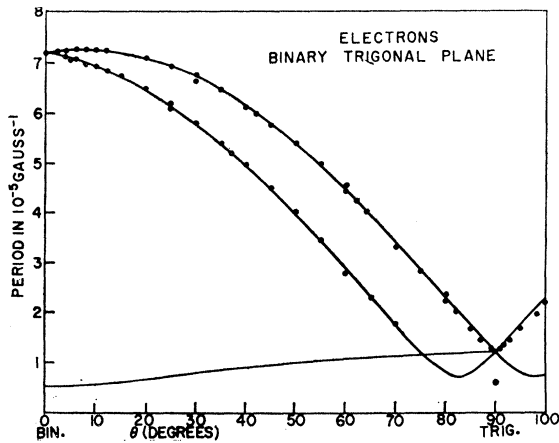


FIG. 7. The electron data in the bisectrix plane. The solid lines are the fit using the ellipsoidal Fermi surface as in Fig. 2. The encircled point along the trigonal direction, of  $P = 0.6 \times 10^{-5} \text{ G}^{-1}$ , is the second-harmonic period observed when the cancellation of the fundamental period occurs (see Sec. III).

from  $\sim 1.5$  to 66 ppm. The dHvA oscillations were studied in the trigonal and bisectrix plane.

Figure 9 shows the data obtained in the trigonal plane where electron periods for all the five samples were observed. The amplitude of the oscillations decreases very rapidly with increased doping, presumably because of the rise in the Dingle temperature, since the mean collision time  $\tau$  decreases by a factor  $\sim 50$ , as shown later

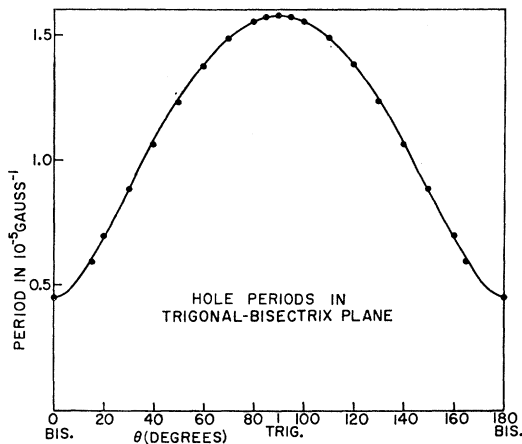


FIG. 8. The data on holes in the binary planes. The solid line is an ellipsoidal fit to the data using the eigenperiods obtained with  $H$  along the three crystal axes.

in Sec. V. Measurements for hole periods in the binary plane were taken for all the samples except alloy 5, as shown in Fig. 10. The hole and electron amplitudes in the trigonal direction in alloy 5 are too small to be observed. The electron periods along the trigonal axis are measured by looking at the intersection of the two branches as shown in case of Bi in Fig. 7. The electron period for alloy 5 in the trigonal direction is however too small to be measured.

The periods  $P_{n,p}$  and the percentage change  $(\Delta P/P)_{n,p}$  for  $H$  in the crystallographic axes for the

various alloys are listed in Table VI. For all the alloys, we observe that the area of the electron ellipsoid decreases by the same percentage ratio in all the directions (Fig. 9). This was also observed by Brandt and Ruzumeenko.<sup>21</sup> For alloy 1 the change  $\Delta P$  for electron

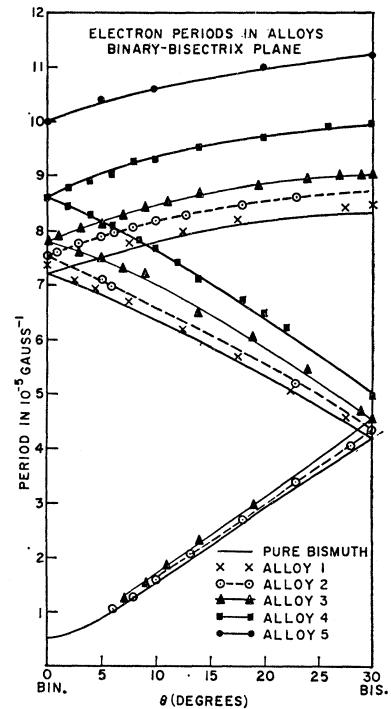


FIG. 9. The angular dependence of the electron periods of various Bi-Pb alloys in the trigonal plane.

period in the trigonal direction is less than the experimental uncertainty.

## IV. RESULTS AND DISCUSSIONS

### A. Bismuth

#### 1. Carrier Density

The data in Figs. 2, 3, and 7 on the electron Fermi surface show that it is well fit by the ellipsoidal model.

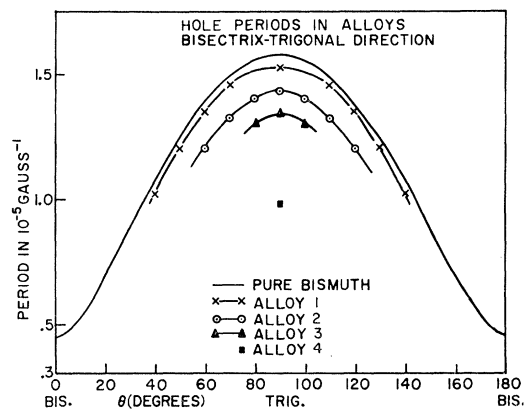


FIG. 10. The angular dependence of hole periods of various Bi-Pb alloys in the binary plane.

The number density for an ellipsoidal Fermi surface is given by

$$n = (8\pi/3)(e/\pi\hbar c)^{3/2}(P_1 P_2 P_3)^{-1/2}, \quad (7)$$

where  $P_1$ ,  $P_2$ , and  $P_3$  are the eigenperiods for the ellipsoids listed in column 3 of Table II. We have obtained the period  $P_3$  along the "3" axis of the ellipsoid (i.e., along the tilt) by extrapolating the ellipsoidal fit. Such an extrapolation leads to a maximum uncertainty of approximately 5% in the determination of  $P_3$ , as estimated from the maximum experimental error existing in the data at  $\pm 5^\circ$  from the tilt angle in Fig. 3. The value of  $n$  obtained is

$$n = 0.96 \pm 0.05 \times 10^{17}/\text{cc}.$$

For the hole ellipsoid we have obtained

$$p = 3.00 \pm 0.10 \times 10^{17}/\text{cc}.$$

We do observe a slight deviation from the ellipsoidal fit ( $\sim 5\%$ ) in the small period branch in the vicinity of the binary direction in Fig. 2. Such a deviation would correspond to an addition of a small volume at the tip of the long cigar-shaped electron ellipsoid (anisotropy  $k_2/k_3 \sim 12.6$ ) and would not increase  $n$  by more than 1%. Hence the stated error in the determination of  $n$  is that due to the uncertainty in fitting the experimental periods to an ellipsoidal model, rather than in deviations from it. The ratio of  $p/n = 3$  within the experimental error. Williams<sup>31</sup> from his measurements on Alfvén wave propagation in Bi, obtained  $N_n = N_p = 3.10 \pm 0.10$ ;  $N$ 's denote the total density of carriers. Combining this with our results shows there to be three electron ellipsoids and one hole ellipsoid, in agreement with the earlier conclusion of Jain and Koenig.<sup>17</sup>

## 2. Effective Mass and Dingle Temperature

The electron effective mass in the binary direction was determined from the temperature dependence of the amplitude as expressed by Eq. (6). Our value  $m^* = 0.011$  coincided with that obtained by cyclotron resonance.<sup>15</sup> Consequently, we felt confident in using the effective masses as determined by cyclotron resonance<sup>15</sup> to determine the Dingle temperatures for other orientations from the field dependence of the amplitudes measured at fixed temperature. The Dingle temperature for holes for  $H$  in the trigonal direction is  $\kappa_p = 0.2^\circ\text{K}$  for  $m^* = 0.067 m_0$ .

For electrons,  $\kappa_n = 0.70^\circ\text{K}$  in the binary direction and  $\kappa_n = 0.65^\circ\text{K}$  at  $9.5^\circ$  from the tilt angle in the binary plane, slightly lower than reported previously.<sup>3</sup> The average values of the collision broadening obtained with the aid of Eq. (4) from the low field galvanomagnetic measurement of Zitter's<sup>32</sup> and holes are, respectively,  $\kappa_n^0 = 0.013^\circ\text{K}$  and  $\kappa_p^0 = 0.005^\circ\text{K}$ . Our samples have a residual resistance somewhat less than Zitter's.

<sup>31</sup> G. A. Williams, Phys. Rev. **139**, A771 (1965).

<sup>32</sup> R. N. Zitter, Phys. Rev. **127**, 1471 (1962).

We observe then, that the collision broadening in the dHvA effect for electron and holes, respectively, is greater than 46 and 40 times the transport result. Shoenberg and Stiles<sup>6</sup> in their dHvA data on potassium observed that the dHvA collision-broadening is 20 times what one expects from resistivity measurements. They attributed this discrepancy to the field-dependent reduction of the dHvA amplitude due to causes other than collision broadening, for instance slight field inhomogeneity over the specimen. However, we expect such variations to be quite small since the interval  $\Delta H$  between the two consecutive dHvA oscillations in Bi is much greater than the field inhomogeneity we have in the electromagnet. We cannot account for the large difference between Dingle temperature, which measured the lifetime in a Landau level and the collision broadening as determined from transport. It would appear that many transitions occur between Landau levels that do not contribute to the resistivity.

We can ascertain the ratio of the amplitudes of holes to electron periods in any direction expected from the difference in Dingle temperatures. For example, in the trigonal direction, the effective mass of the holes is essentially the same as that of the electrons from Eq. (3) then

$$\begin{aligned} \left| \frac{(dI/dH)_n}{(dI/dH)_p} \right|_{\text{trig}} &= \exp \left[ \frac{4\pi^3 m^* k c (\kappa_p - \kappa_n)}{e h H} \right] \\ &= 1/20 \quad \text{for } H \sim 3.3 \text{ kG}. \end{aligned}$$

The analysis shows why it is difficult to observe any electron periods in the trigonal direction. We were only able to observe the electron periods from  $H$  in the trigonal direction by eliminating the contribution from the holes, as discussed earlier.

## 3. Band Structure

(a) *Electrons.* It is quite clear from the foregoing discussion that the electron Fermi surface in bismuth can be very well described by three equivalent highly eccentric ellipsoids in momentum space, that one principal axis of each ellipsoid is parallel to a crystal axis of the twofold rotational symmetry (the binary axis) and that the other two principal axes are tilted about  $6.5^\circ$  from the trigonal and bisectrix axis. However, the form of the energy momentum dispersion  $E(\mathbf{p})$  has been the subject of some recent controversy. In 1939 Shoenberg<sup>3</sup> proposed a simple parabolic model for the tilted ellipsoid for which, in the principal axis system of the ellipsoid, the dispersion relation is given by

$$\frac{p_1^2}{2m_1} + \frac{p_2^2}{2m_2} + \frac{p_3^2}{2m_3} = E. \quad (8)$$

Shoenberg,<sup>3</sup> from the periods and the temperature variation of the amplitude of the dHvA oscillations, ob-

tained the values of energy independent components of the mass tensor:  $m_1=0.0049 m_0$ ,  $m_2=1.20 m_0$ ,  $m_3=0.012 m_0$ , and  $E=17.7$  meV.

The existence of such a small mass means that there is an interaction with another band (or other bands) from the sum rule for the effective mass. Lax and collaborators<sup>11</sup> from magneto reflection experiment on Bi deduced that in fact the energy gap between the conduction and valence bands is small ( $\sim 15$  meV) and that the Fermi level lies in the nonparabolic region of the conduction band. The deviation from parabolic behavior for an isotropic surface in the vicinity of a small band gap was derived by Kane<sup>33</sup> for In Sb. Lax,<sup>11</sup> modifying Kane's results for Bi, proposed a nonparabolic dispersion

$$\frac{p_1^2}{2m_1} + \frac{p_2^2}{2m_2} + \frac{p_3^2}{2m_3} = E(1 + E/E_\theta), \quad (9)$$

where 1, 2, and 3 refer to the principal axis of the ellipsoids and the  $m$ 's are the effective masses at the bottom of the conduction band. The surfaces of constant energy for this model are clearly ellipsoidal; we shall, therefore, refer to this model as ellipsoidal nonparabolic (ENP). The criterion for the validity of Eq. (9) is that all three principal components of  $m$  be small, because of a single small gap.

Cohen<sup>16</sup> pointed out that since the effective mass component  $m_2 \sim m_0$  the dispersion relation should be parabolic in the 2 direction. Cohen's calculations for minima at the  $L$  points in the Brillouin zone give

$$\frac{p_1^2}{2m_1} + \frac{p_2^2}{2m_2} + \frac{p_3^2}{2m_3} = E(1 + E/E_\theta) - \frac{1}{E_\theta} \left( \frac{p_2^2}{2m_2} \right)^2 \quad (10)$$

which differs from Eq. (9) only by the right-hand term. This expression has a nonparabolic dispersion in the 1 and 3 directions and is parabolic along 2. The resulting constant energy surfaces are nonellipsoidal; the model will be referred to as NENP. Weiner<sup>14</sup> in dHvA studies in Bi and Bi-Te alloys and Kao<sup>15</sup> in cyclotron resonance of Bi used the NENP model to interpret their data. In the work of Kao,<sup>15</sup> where  $E=22$  meV and  $E/E_\theta=0.5$  were used, and in the subsequent recomputation of this data by Kao *et al.*<sup>23</sup> using  $E=25$  meV and  $E/E_\theta=5/3$ , he derived a value for  $n$  which is 30% too large, using the NENP model. The only experimental data involved are the cyclotron masses. The discrepancy is such as to suggest that the NENP model yields an integrated volume in  $k$  space that is too large. Weiner's work is insensitive to the difference between the two models.

Since the cyclotron mass  $m^*$  measures the rate of change of area  $S$  with energy, the ratio  $S/m^*$  give the curvature of the energy-momentum surface. Combining the present measurements of  $S$  with the measured values of  $m^*$ ,<sup>15</sup> and comparing  $(S/2\pi m^*)$  so obtained with the values computed on the basis of the known

TABLE III. Variation of  $\eta$  [Eq. (14)] and  $S/2\pi m^*$  [Eq. (11)] with  $E/E_\theta$ .

$E/E_\theta$	$\eta$	$(S/2\pi m^*)^{\text{ENP}}$	$(S/2\pi m^*)^{\text{ENP}}$ for $E=25$ meV	$(S/2\pi m^*)^{\text{ENP}}$ for $E=27$ meV
1	1.18	0.667E	16.7	18.0
5/3	1.19	0.615E	15.4	16.6
9/5	1.22	0.609E	15.2	16.4
2	1.23	0.600E	15.0	16.2

models of electron Fermi surface, we are able to (i) decide about the probable nature of the dispersion relation and (ii) obtain the values of Fermi energy  $E$  and the energy gap  $E_\theta$ .

The ENP model gives the same result for all directions of the magnetic field:

$$\left( \frac{S}{2\pi m^*} \right)_{1,2,3}^{\text{ENP}} = \frac{E(1 + E/E_\theta)}{(1 + 2E/E_\theta)}. \quad (11)$$

Cohen's model gives

$$\left( \frac{S}{2\pi m^*} \right)_2^{\text{NENP}} = \frac{E(1 + E/E_\theta)}{(1 + 2E/E_\theta)} \quad (12)$$

and

$$\left( \frac{S}{2\pi m^*} \right)_{3,1}^{\text{NENP}} = \eta \frac{E(1 + E/E_\theta)}{(1 + 2E/E_\theta)}, \quad (13)$$

where (in Kao's<sup>15</sup> notation)

$$\eta = \frac{4b^{1/2}}{(b^{1/2} + \frac{1}{2})} \left( \frac{I}{K} \right), \quad (14)$$

$$I = \left[ \frac{1-k^2}{k^2} K(k) - \frac{1-2k^2}{k^2} \epsilon(k) \right],$$

$$k^2 = (b^{1/2} - \frac{1}{2}) / 2b^{1/2},$$

$$b = \{ E/E_\theta(1 + E/E_\theta) + \frac{1}{4} \},$$

and  $K(k)$  and  $\epsilon(k)$  are the elliptic integrals of the first and second kinds. Combining Eqs. (12) and (13)

$$\left( \frac{S}{2\pi m^*} \right)_{1,3}^{\text{NENP}} = \eta \left( \frac{S}{2\pi m^*} \right)_2^{\text{NENP}}. \quad (15)$$

Thus  $\eta \neq 1$  will indicate different dispersion in different directions.

From the results tabulated in Table III, we note that the deviation of  $(S/2\pi m^*)_{3,1}^{\text{NENP}}$  from  $(S/2\pi m^*)_2^{\text{NENP}}$  is of the order of 20%. From the last column of Table II, we note that the measured value of  $(S/2\pi m^*)_{3,1}$  does not differ from  $(S/2\pi m^*)_2$  by more than 2% with maximum uncertainties in the determination of  $S$  and  $m^*$ , however, of 5% and 10%, respectively. Thus the factor  $S/2\pi m^*$  is constant for all direction within the experimental uncertainties, and  $\eta$  is unity. This is a strong argument for disregarding the NENP model, for which

<sup>33</sup> E. O. Kane, J. Phys. Chem. Solids 1, 249 (1957).

TABLE IV. Comparison of various values of the Fermi and gap energies in meV.

Energy meV	Brown <i>et al.</i> <sup>a</sup>	Engeler <sup>b</sup>	Weiner <sup>c</sup>	Hebel and Wolff <sup>d</sup>	Brandt <i>et al.</i> <sup>e</sup>	Grenier <i>et al.</i> <sup>f</sup>	Smith <i>et al.</i> <sup>g</sup>	Esaki and Stiles <sup>h</sup>	Present
$E_n$	25	22	22	27	23	...	27.6	15	25.0
$E_g$	15	24	46	15	...	...	15.3	20	15.0
$E_p$	...	...	11.8	...	11.2	11.9	10.9	15	11.0

<sup>a</sup> See Ref. 12.<sup>b</sup> See Ref. 13.<sup>c</sup> See Ref. 14.<sup>d</sup> See Ref. 34.<sup>e</sup> See Ref. 29.<sup>f</sup> G. G. Grenier, J. M. Reynolds, and J. R. Sybert, *Phys. Rev.* **132**, 58 (1963).<sup>g</sup> G. E. Smith, G. A. Baraff, and I. M. Rowell, *Phys. Rev.* **135**, A1118 (1964).<sup>h</sup> L. Esaki and P. J. Stiles, *Phys. Rev. Letters* **14**, 902 (1965).

$\eta=1.20$ . The other alternative is the ENP model, for which  $\eta=1$  from Eq. (11). From Table II, the experimental value of  $S/2\pi m^*$  is 15.4. To obtain this value from the ENP model requires  $E/E_g=5/3$ , as shown in Table III. Then  $E=25.0$  meV and  $E_g=15.0$  meV. These values of the Fermi and gap energies are in good agreement with previously reported values (Table IV). (With respect to the results of Hebel and Wolff<sup>34</sup> in Table IV, however, though they find that  $E=27$  meV fits their data significantly better than  $E=25$  meV, we would require  $E_g=8.8$  meV were  $E=27$  meV.) The ENP model, considered as an empirical model, describes the conduction band very well. As shown later it is also compatible with our data on Bi-Pb alloys, in which we observe that the areas of the ellipsoids shrink at the same rate in all directions. Thus we conclude that the same dispersion curve holds for electrons in all directions.

There occurs some small deviation from the ellipsoidal model in the region within 5% of the binary axis for the small period branch in Fig. 2. This deviation could either be attributed to some small nonellipsoidal present or to the fluctuation of the Fermi energy as a function of the magnetic field. The latter effect, due to a fractional change in the Fermi energy  $E_F$  whenever Landau bands go through the Fermi surfaces, contributes only when  $E_F/\hbar\omega_c$  approaches unity  $\omega_c$  being the cyclotron frequency. In the range of measurements of 1 to 10 kG,  $E_F/\hbar\omega_c > 1$  for this particular electron ellipsoid and this effect could be neglected. We attribute this small deviation then to the presence of non-ellipsoidal. Such a small deviation from an ellipsoidal model was recently reported by Edelman and Khaikin<sup>35</sup> in their measurements of the cyclotron resonance in Bi. In order to reconcile the two facts that the dispersion should be the same in all directions and a certain amount of nonellipsoidal should be present, one should somewhat modify NENP model and possibly include some additional term. This has been also pointed out by Dimmock<sup>36</sup> who showed that Cohen neglected some terms in deriving Eq. (10), which are comparable to

<sup>34</sup> L. C. Hebel and P. A. Wolff, *Phys. Rev. Letters* **11**, 517 (1963).<sup>35</sup> V. S. Edelman and M. S. Khaikin, *Zh. Eksperim. i Teor. Fiz.* **49**, 107 (1965) [English transl: *Soviet Phys.—JETP* **22**, 77 (1966)].<sup>36</sup> J. O. Dimmock, Lincoln Laboratory Reports (MIT) No. 1, 1964, p. 41 (unpublished).

some of the terms already present in Eq. (10); and that a more general dispersion relation should be used. In the main, however, the small deviations from an ellipsoidal Fermi surface contributes only  $\sim 1\%$  to the density of states. What is significant is that the energy dispersion in the heavy mass direction in  $k$  space is as great as in the light mass direction.

(b) *Holes*. The hole Fermi surface is Bi is traditionally described by the parabolic dispersion relation

$$\beta_1 p_x^2 + \beta_2 p_y^2 + \beta_3 p_z^2 = 2m_0 E_p,$$

where  $\beta$ 's are the components of the hole inverse mass tensor and the measured values due to Kao<sup>15</sup> are  $\beta_1=\beta_2=14.8$  and  $\beta_3=1.32$ . Since  $\beta$ 's are small, the deviation from parabolic behavior should be small on the basis of the  $\mathbf{k}\cdot\mathbf{p}$  approximation. In what follows we shall consider the parabolic dispersion relation for the hole band.

The dHvA data as shown in Fig. 8 agree well with the ellipsoidal surface. The speculation of Brandt *et al.*<sup>37</sup> that the hole Fermi surface may deviate from ellipsoidal shape is inconsistent with our data. The Fermi energy  $E_p$  for holes is  $E_p=(e\hbar/m^*c)1/P$ . For  $\mathbf{H}\parallel 3$ ;  $P=1.575 \times 10^{-5}$  G<sup>-1</sup> and  $m^*=0.067$  which gives a Fermi energy  $E_p=11.0$  meV. As shown in Table IV, this is in good agreement with the earlier measurements.

## B. Bismuth-Lead Alloys

Since the ENP model seems appropriate for the conduction band of pure Bi, we shall use it to compute the relevant parameters in Bi-Pb alloys. The area  $S_i$  of the ellipsoid normal to a direction  $i$  is

$$S_i = C_i E (1 + E/E_g), \quad (16)$$

where  $C_i$  involves the masses at the bottom of the band. Expanding about the Fermi energy, assuming  $E_g$  constant, gives (exactly):

$$\left(\frac{\Delta S}{S}\right)_n = \frac{(1+2E/E_g)}{(1+E/E_g)} \left(\frac{\Delta E}{E}\right)_n - \frac{E/E_g}{1+E/E_g} \left(\frac{\Delta E}{E}\right)_n^2 \quad (17a)$$

with

$$(\Delta S/S)_n = \{1 - (1 + |\Delta P/P|_n)^{-1}\}. \quad (17b)$$

<sup>37</sup> N. B. Brandt, A. E. Dubrovskaya, and G. A. Kytin, *Zh. Eksperim. i Teor. Fiz.* **37**, 572 (1959) [English transl: *Soviet Phys.—JETP* **10**, 405 (1960)].

TABLE V. dHvA data on Pb-doped Bi alloys.

Alloys \ Axis	Periods in $10^{-5}$ G $^{-1}$ and $ \Delta P/P $ in %				Holes Trigonal	$(\Delta S/S)_n$ %	$(\Delta S/S)_p$ %	$\Delta E_n$ meV	$\Delta E_p$ meV	$\Delta E = \Delta E_p - \Delta E_n$ meV
	Bisectrix	Binary	Trigonal	Average						
Pure Bi	8.30	7.20	1.17		1.575					
Alloy 1	8.45	7.33	$\sim 1.19$		1.52					
	1.81	1.80	$\sim 1.7$	1.8	3.5	2.0	3.6	0.32	0.40	0.08
Alloy 2	8.70	7.55	1.22		1.43					
	4.82	4.86	4.27	4.65	9.2	4.6	10.1	0.73	1.01	0.28
Alloy 3	9.00	7.80	1.25		1.34					
	8.40	8.30	6.80	7.83	14.9	7.4	17.5	1.18	1.93	0.75
Alloy 4	9.94	8.6	1.4		1.0					
	19.9	19.4	19.6	19.6	36.5	16.0	57.4	2.58	6.31	3.83
Alloy 5	11.2	10.0	...	...	...					
	34.9	38.9	...	36.9		27.0		4.45		

The change in hole Fermi energy is given by

$$(\Delta E/E)_p = (\Delta S/S)_p = \{1 - |\Delta P/P|_p\}^{-1}, \quad (18)$$

where  $\Delta P/P = (P_{\text{alloy}} - P_{\text{Bi}})/P_{\text{Bi}}$ , and similarly for  $\Delta S/S$ . From Fig. 11, we note that the areas of the electron ellipsoids decrease with doping by the same percentage ratio in all directions, showing that the ENP model should remain an appropriate model for the conduction band of the alloys. Taking the average  $|\Delta P/P|_n$  and  $|\Delta P/P|_p$  as listed in Table V, we compute the Fermi energy shift  $\Delta E_n$  and  $\Delta E_p$  by using Eqs. (17a), (17b), and (18); the value of the Fermi energies used are  $E_n = 25.0$  meV and  $E_p = 11.0$  meV. The changes in the overlap  $\Delta E = (\Delta E_p - \Delta E_n)$  are listed in the last column of Table V. From the values of  $\Delta E$  for the various alloys we conclude that the overlap of the conduction and valence bands does not change appreciably. The movement noticed in alloy 4 may be attributed to the uncertainty in the determination of the low-amplitude dHvA period for holes. Thus the conduction band and the overlapping valence neither change their shape nor their relative position, under light doping.

If  $\Delta n$  and  $\Delta p$  denote the change in the electron and hole concentrations per ellipsoid, respectively, then the total change in number of carriers  $\Delta$  is given by

$$\Delta = 3\Delta n + \Delta p \quad (19)$$

as there are three electron ellipsoids and one hole

ellipsoid. Using Eq. (7), we have

$$\begin{aligned} \Delta n/n &= 1 - (1 + |\Delta P/P|_n)^{-3/2}, \\ \Delta p/p &= (1 - |\Delta P/P|_p)^{-3/2} - 1. \end{aligned}$$

Using our values  $n$ ,  $p$ , and  $|\Delta P/P|$ 's we obtain the value of  $\Delta$  as listed in Table VI. If  $N_{\text{Pb}}$  is the number of Pb atoms contributing a unit difference in the electron and hole concentration, then  $N_{\text{Pb}} = n_0 C/\Delta$ , where  $n_0 = 3.2 \times 10^{22}/\text{cc}$  is the number of Bi atoms/cc and  $C$  is the concentration of Pb in Bi as determined by quantitative emission spectroscopy.<sup>25</sup> The average value of  $N_{\text{Pb}}$  is found to be 1.86 in contrast to 55 atoms of Pb contributing one electron obtained by Brandt *et al.*<sup>21</sup> On the basis of rigid bands, one would expect  $N_{\text{Pb}} = 2$ , in agreement without measured value.

## V. GALVANOMAGNETIC RESULTS ON Bi-Pb ALLOYS

The value of the carrier concentration  $\Delta$  can be obtained, without dHvA effect, by a study of the resistivity and Hall coefficient as a function of magnetic field. It was originally hoped that the galvanomagnetic measurements would serve as an independent check on  $\Delta$ . However, the dHvA values turned out to be more accurate. Combining then our dHvA and galvanomagnetic data, the electron and hole mobility can be obtained. A simple analysis for moderate magnetic fields and low tempera-

TABLE VI. Results on Pb-Bi alloys.

Alloys	Conc. of Pb in ppm		$3\Delta n$ $10^{15}/\text{cc}$	$\Delta p$ $10^{15}/\text{cc}$	$\Delta = 3\Delta n + \Delta p$ $10^{15}/\text{cc}$	$N_n$ $10^{17}/\text{cc}$	$N_p$ $10^{17}/\text{cc}$	$N_{\text{Pb}} = n_0 C/\Delta$
	$C_0^a$	$C^b$						
1	12	$\sim 1.5$	9.0	16.5	25.5	2.91	3.16	1.88
2	90	3.5	20.0	46.8	66.8	2.80	3.47	1.68
3	230	7.7	32.0	82.2	114.2	2.68	3.82	2.14
4	520	22	70.8	292.8	363.6	2.29	5.93	1.93
5	800	66	112.5	1170.0	1282.5	1.87	15.83	1.64
Average $N_{\text{Pb}} = 1.86$								

<sup>a</sup> The concentration of Pb assuming unity segregation coefficient.

<sup>b</sup> The amount of Pb estimated by quantitative emission spectroscopy.

TABLE VII. Results of the galvanomagnetic data on Pb-Bi alloys.

Alloy	$\Delta_{\text{Hall}}$ $10^{15}/\text{cc}$	$a$	$b$	Measured mobilities		Corrected mobilities		Effective $\Delta$	
				$\mu_p^0 = 1.2 \times 10^7$ $\text{cm}^2/\text{Vsec}$	$\mu_n^0 = 4.2 \times 10^7$ $\text{cm}^2/\text{Vsec}$	$\mu_p$ $\text{cm}^2/\text{Vsec}$	$\mu_n$ $\text{cm}^2/\text{Vsec}$	Electrons $10^{15}/\text{cc}$	Holes $10^{15}/\text{cc}$
Alloy 1	25	$1.8 \times 10^6$	$1.2 \times 10^{12}$	$1.0 \times 10^6$	$1.2 \times 10^7$	$1.1 \times 10^6$	$1.7 \times 10^7$	26	64
Alloy 2	70	$1.9 \times 10^6$	$2.7 \times 10^{12}$	$3.7 \times 10^5$	$5.4 \times 10^6$	$3.8 \times 10^5$	$6.2 \times 10^6$	69	150
Alloy 3	123	$5.5 \times 10^6$	$3.7 \times 10^{12}$	$2.4 \times 10^5$	$3.8 \times 10^6$	$2.44 \times 10^5$	$4.2 \times 10^6$	121	240
Alloy 4	328	$1.0 \times 10^8$	$19.3 \times 10^{12}$	$5.9 \times 10^4$	$1.2 \times 10^6$	$5.9 \times 10^4$	$1.23 \times 10^6$	415	624
Alloy 5	1176	$3.7 \times 10^9$	$99 \times 10^{12}$	$2.0 \times 10^4$	$3.2 \times 10^5$	$2.0 \times 10^4$	$3.2 \times 10^5$	1655	1552

tures is possible if the trigonal axis is parallel to  $H$ . If  $H$  is chosen such that  $\mu H \ll 1$ , but not so large that the quantum effects become important the binary resistivity  $\rho_{xx}$  and Hall coefficient  $R$  can be combined to give<sup>38</sup>

$$\rho_{xx}^{-1} = e \left( \frac{b^2 - 2\Delta a}{b} \right) \frac{1}{H^2} + \frac{\Delta^2 e}{b}, \quad (20)$$

$$\frac{R}{\rho_{xx}} = -\frac{a}{b} \left( \frac{1}{H^2} \right) + \frac{\Delta}{b}, \quad (21)$$

where

$$a = -N_n/\mu_1\mu_2^* + N_p/\mu_p^2, \quad (22)$$

$$b = N_n\bar{\mu}/\mu_1\mu_2^* + N_p/\mu_p. \quad (23)$$

Here  $N_n$  and  $N_p$  are the total concentration free electrons and holes;  $\bar{\mu} = (\mu_1 + \mu_2^*)/2$  is the average of the mobilities of the electrons in the trigonal plane;  $\mu_p$  is the mobility of holes in that plane;  $\mu_1$ ,  $\mu_2$ , and  $\mu_3$  are the mobilities in the principal direction of each ellipsoid;  $\mu_2^* = \mu_2 \cos^2 \theta_i + \mu_3 \sin^2 \theta_i$ , where  $\theta_i$  is the tilt angle. Plotting  $\rho_{xx}^{-1}$  versus  $H^{-2}$  and  $R/\rho_{xx}$  versus  $H^{-2}$  should yield straight lines. The extrapolation of the linear region of Eqs. (20) and (21) between 2 and 5 kG gives intercepts  $\Delta^2/b$  and  $\Delta/b$ , respectively. The ratio of the two intercepts yields  $\Delta$  directly. These values of  $\Delta$ , listed in Table VII, though less accurate, agree well with the ones obtained from dHvA effect. With the knowledge of  $\Delta$ , slope, and intercept of Eq. (20), we compute the value of  $a$  and  $b$ . In order to calculate the mobilities  $\mu_1$  and  $\mu_p$  from  $a$  and  $b$ , we must know  $N_n$ ,  $N_p$ , and the ratio  $\mu_1/\mu_2^*$ . Zitter<sup>32</sup> has shown from his low-field galvanomagnetic measurements that the relaxation time tensor  $\tau$  is nearly isotropic. We shall assume that  $\tau$  is isotropic in the alloys as well; i.e., that the mobility anisotropy is given by the mass anisotropy which, from the data, does not change on alloying. With Zitter's value of  $(\mu_1/\mu_2^*)_{\text{Bi}}$  and the value of  $N_n$  and  $N_p$  from our dHvA data we compute  $\mu_1$  and  $\mu_p$  from Eqs. (22) and (23) listed in Table VII.

The main scattering mechanism we need be concerned with is that due to ionized impurities. To obtain the contribution of the ionized impurity scattering to the mobility, we subtract the intrinsic scattering rate from

<sup>38</sup> B. H. Schultz and J. M. Noothoven van Goor, Philips Res. Rept. 19, 103 (1964).

the total rate. If  $\mu_1$  and  $\mu_{\text{Bi}}$  are the mobilities for alloy and pure metal, respectively, the ionized scattering mobility  $\mu_n$  is given by

$$\mu_n = \mu_1 / (1 - \mu_1/\mu_{\text{Bi}});$$

a similar expression holds for holes. The values of  $\mu_{\text{Bi}}$  for electrons and holes used are  $4.2 \times 10^7$   $\text{cm}^2/\text{V sec}$  and  $1.2 \times 10^7$   $\text{cm}^2/\text{V sec}$  as obtained by Zitter<sup>32</sup> at 4.2°K.

To explain the ionized impurity scattering, two extreme cases have been discussed in the literature according as whether  $kR \gg 1$  or  $kR \ll 1$ , where  $k$  is the carrier wave number and  $R$  the range of the scattering potential. For our case,  $kR \gg 1$ , as shown later. This case has been discussed for the semiconductors by Conwell and Weisskopf<sup>39</sup> who used the Rutherford scattering formula cut off for small angle scattering and independently by Brooks and Herring,<sup>40</sup> and Dingle<sup>41</sup> who use the Born approximation and a screened Coulomb field. The most appropriate computation for our case is that of Dingle,<sup>41</sup> who also considered the simultaneous presence of holes and electrons in degenerate semiconductors.

Under Thomas-Fermi screening, it is well known that

$$U = (e^2/Kr)e^{-r/R}$$

is the potential of an electron in the field of a screened singly ionized impurity,  $K$  being the dielectric constant of the medium and  $R$  the screening radius. If holes and electrons are both present, the screening radius for the degenerate system is given by

$$R^{-2} = (4\pi e^2/K) \{n(\epsilon_n) + n(\epsilon_p)\},$$

where  $n(\epsilon)$ 's are the density of states of the particular carrier at the Fermi energy. For a parabolic dispersion law  $n(\epsilon) = \frac{3}{2}(N/\epsilon)$ , where  $N$  is the total number of the particular carrier and  $\epsilon$  is the density of states energy." For pure Bi,  $\epsilon_n = 15.4$  meV,  $\epsilon_p = 11.0$  meV, and  $N_n = N_p = 3.0 \times 10^{17}/\text{cc}$ . Using these values we obtain  $R^{-2} = 0.80 \times 10^{12}$   $\text{cm}^{-2}$ . The value of  $R^{-2}$  does not change by more than 2% from pure Bi to the highest Pb-doped sample.

<sup>39</sup> E. M. Conwell and V. F. Weisskopf, Phys. Rev. 69, 258 (1946); 77, 388 (1950).

<sup>40</sup> Cf. P. P. Debye and E. M. Conwell, Phys. Rev. 93, 693 (1954).

<sup>41</sup> R. B. Dingle, Phil. Mag. 46, 831 (1955).

Dingle's expression for the relaxation time is

$$\tau = \frac{K^2 m^{*2} v^3}{2\pi N_i e^4} \left\{ \ln(1+\xi) - \frac{\xi}{1+\xi} \right\}, \quad (24)$$

where  $m^*$  is the isotropic effective mass and  $v$  the Fermi velocity of the carrier,  $N_i$  the number of scattering centers,  $K$  the dielectric constant, and  $\xi = 4k^2 R^2$ .  $\xi$  is a measure of the ratio of the range of the scattering potential  $R$  to the de Broglie wavelength of the carrier. Using the values of  $R$  and  $k$  we obtain  $\xi_n = 102.0$  and  $\xi_p = 31.0$ . For pure Bi, since  $\xi \gg 1$ , we can approximate the expression  $\{\ln(1+\xi) - \xi/(1+\xi)\}$  by  $(\ln\xi - 1)$  in Eq. (24).

The dependence of the mobility  $\mu_n$  on the number of scattering centers is then given by

$$\mu_n \sim \frac{E_n (E_n/m^*)^{1/2}}{N_i (\ln\xi_n - 1)}. \quad (25)$$

For electrons, if we use the relation between  $m^*$  and  $E$  as derived on the basis of Eq. (9),  $m^*$  being the mass in the binary direction, we note that the factor within the bracket in Eq. (25), does not change by more than 2% from one alloy to another. For all practical purposes we can neglect the variation of this for electrons. Since the number of scattering centers is some constant multiple of  $\Delta$  we can plot  $\log\mu$  versus  $\log(\Delta_{\text{eff}}^{-1})$ , where  $\Delta_{\text{eff}}^{-1} = \Delta^{-1} E_n$ . The plot showed in Fig. 11 is a straight line of slope approximately  $-1.0$ . Thus Eq. (25) qualitatively explains the variation of  $\mu$  with the number of scattering centers.

For holes,  $m^*$  is independent of energy, we have

$$\mu_p \sim \frac{(E_p)^{3/2}}{N_i (\log\xi_p - 1)}. \quad (26)$$

Figure 11 shows the plot  $\mu_p$  versus  $\log\Delta_{\text{eff}}$ , where  $\Delta_{\text{eff}} = \text{const} \times N_i (\log\xi_p - 1) / E_p^{3/2}$ . The slope of the line is  $-1.2$ . Since  $\xi = 4k^2 R^2$  we note that  $(kR)_n = 5.0$  and  $(kR)_p = 2.8$  for pure Bi. As  $kR \sim 1$  for holes, the Born approximation is not very good. This may be the reason that the straight line for holes in Fig. 11 deviates from a slope of 1.0.

## VI. CONCLUSION

It is confirmed that in Bi, the electron Fermi surface consists of three ellipsoids which are very well described

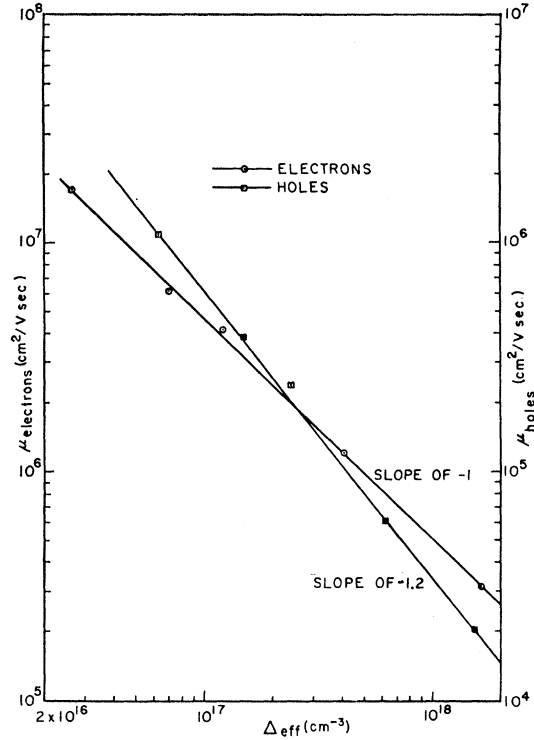


FIG. 11. The variation of electron and hole mobilities as a function of doping.  $\Delta_{\text{eff}}$  is related to  $\Delta$  as defined in the text.

by an ellipsoidal, nonparabolic dispersion relation, and that any nonellipsoidality present is small; the hole Fermi surface is ellipsoidal. From the studies of lightly Pb-doped Bi alloys it is established that Pb acts as a single valence acceptor, and that for these low dopings band edges do not move with respect to other. The mobilities in these alloys are dominated by the ionized impurity scattering.

## ACKNOWLEDGMENTS

The author would like to thank Dr. Seymour H. Koenig for suggesting the present investigation and for his continued guidance and encouragement throughout the work; Rodney D. Brown, Walter Schillinger, Robert L. Hartman, and Alberto A. Lopez for their help and stimulating discussions, Dr. W. Reuter of IBM Research Center, Yorktown Heights, for performing the spectroscopic analysis on the Pb-doped Bi samples, and many other members of the Watson staff who were of invaluable assistance.